Citation:
Miguel M. Moreira, Guilherme Ramos, Rui Henriques, 2025
Actionable Brain Maps of Transcriptional Regulation of Neurotransmission Activity from Postmortem Cohorts
In INForum - Bioinformatics Track, September 2025, Évora, Portugal

Actionable Brain Maps of Transcriptional Regulation of Neurotransmission Activity from Postmortem Cohorts

Miguel M. Moreira[1,2,4], Guilherme Ramos[2,3], and Rui Henriques[1,2,*]

[1]INESC-ID, Portugal
[2]Instituto Superior Técnico, Universidade de Lisboa, Portugal
[3]Instituto de Telecomunicações, Portugal
[4]LASIGE and Faculdade de Ciências, Universidade de Lisboa, Portugal
{miguelmatamoreira,guilherme.ramos,rmch}@tecnico.ulisboa.pt

Abstract. Transcriptional activity in the human brain is characterized by highly specialized gene expression programs across distinct regions and neurotransmission systems. Despite substantial neuroscientific efforts to model tissue-specific transcriptomic signatures in the brain, there is still a lack of translational tools and actionable maps that consolidate existing knowledge and facilitate the exploration of regulatory activity across different brain regions, demographics, and clinical states. To address this gap, this work proposes a web-based analytical tool that leverages multi-tissue postmortem cohort data from GTEx initiative to model brain transcriptomics through contrasts against peripheral tissues. The tool incorporates demographic and agonal covariates. A novel and principled data-centric methodology is introduced for information summarization, combining statistical frameworks for multi-tissue differential expression testing with pattern discovery techniques (biclustering and triclustering) to identify modular regulatory patterns. Validation against biological networks confirms the tool's relevance for knowledge discovery and reveals novel putative associations in neurotransmission regulation.

Keywords: Brain transcriptomics · Pattern discovery · Neurotransmission
Software: available at `https://github.com/miguelmatamoreira/sdnm`

1 Introduction

Modeling the spatial distribution of neurotransmission markers in the human brain involves identifying actionable maps of differential expression across tissues, taking into account individual psychodemographic traits. Despite the relevance of neurotranscriptomic maps for knowledge acquisition, several factors challenge their learning: i) the variability of gene expression between individuals and presence of critical covariates such as demographic, genotypic, and clinical factors [9]; ii) the lack of *in vivo* data in humans due to the difficulty of accessing brain tissues; or iii) the need for information summarization and visualization approaches with solid guarantees of statistical significance and usability. Advances in technology, including spatial transcriptomics [9], have driven significant development and progress in this field [8]. Despite their relevance, they generally

disregard the value of confounding factors or the role of contrast tissues, such as peripheral tissues, to isolate specific regulatory aspects of the human brain.

This work proposes a methodology to learn actionable maps that offer a structured view of neurotranscriptional activity, using multi-tissue postmortem data from the Genotype-Tissue Expression (GTEx) initiative [1]. The target maps statistically summarize relevant gene-centric and modular regulatory activity at different brain tissues in both the absence and presence of co-factors, such as psychodemographic profile and agonal states (i.e., death circumstances).

To this end, we introduce a novel and principled methodology, combining a statistical framework for rigorous multivariate analysis of differential gene expression at varying tissues and conditions, and pattern discovery, including biclustering and triclustering, for acquiring modular stances on regulatory activity. Further, the information is aided by known functions present in pathway repositories and ontologies, as well as putative functions derived from functional enrichment analysis of coexpression patterns.

We showcase the relevance of the produced maps for expanding the existing knowledge by taking a closer look at genes with well-established or putative roles in neurotransmission systems, specifically receptor-coding genes, given their relevance to understanding brain functions, studying neuropsychiatric diseases, assessing psychopharmacological action, and shaping neuromodulation protocols.

2 Data profiling

To establish the target maps of neurotranscriptomic activity, multi-tissue RNA sequencing data were acquired from GTEx post-mortem cohorts (version 8). In particular, we consider expression data from 18 distinct brain tissues listed in Fig. 1, as well as 4 peripheral tissues: whole blood, adipose tissue, skin (not sun exposed), and skin (sun exposed).

A total of $56,200$ genes were profiled for 931 individuals. The distribution of sex, age, and agonal state of the target population is presented in Fig. 2.

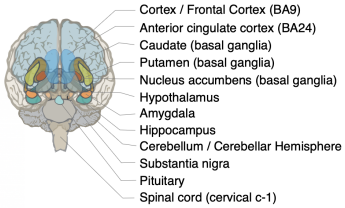

Fig. 1: Brain tissues visually represented [1].

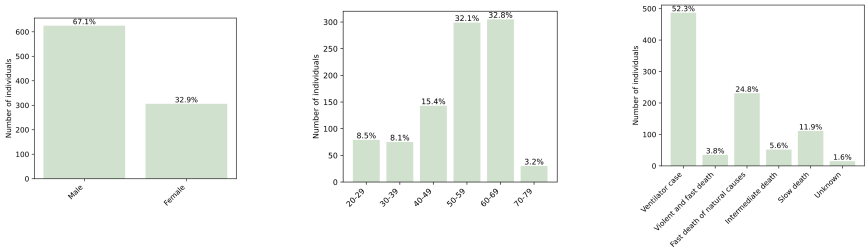

(a) sex (b) age (c) agonal state

Fig. 2: Distribution of demographic and agonal features for the profiled population.

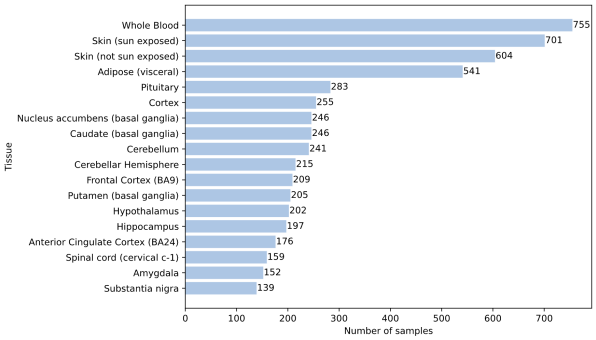

Fig. 3: Number of available samples (individuals) per peripheral and brain tissue.

Not all subjects were subjected to the same site sampling protocol, leading to variations on the amount of available observations per tissue as shown in Fig. 3.

3 Solution

3.1 Data preprocessing

RNA counts are *normalized* as transcripts per million and *log-transformed*.

To establish actionable summaries of the neurotranscriptional activity from the multi-tissue log-transformed RNA data, two major conditions are asserted: brain-specificity by contrasting regulatory activity in brain tissues against peripheral tissues; and tissue-specificity by contrasting regulatory activity at different brain sites.

Statistical tests are conducted to determine whether the expression of a given gene exhibits significant differences between two or more tissues from paired individuals with available samples at the tested sites. To this end, the normality of tissue-conditional gene expression is assessed using the Shapiro-Wilk test at a significance level of 0.05. If normality is rejected, Wilcoxon signed-rank tests for the pairwise testing of differential expression between tissues, and Friedman tests are applied for multi-wise testing in the presence of more than two tissues. Otherwise, t-test and ANOVA are respectively applied.

To produce the *summaries* of transcriptional activity, genes are ranked in accordance with their degree of brain specificity (contrast against peripheral tissues) and site specificity (differentiation across brain regions) using integrative scores, such as the *reciprocal rank fusion*.

To support *filtering* options based on relevant factors such as demography and agonal states, metadata files[1] are sourced from GTEx to create covariates.

To support with the *categorization* of genes according to their roles in key neurological processes, particularly those associated with specific neurotransmission systems, gene descriptors from humans (homo sapiens) were retrieved from

[1] GTEx website (`https://gtexportal.org/home/downloads/adult-gtex/bulk_tissue_expression`)

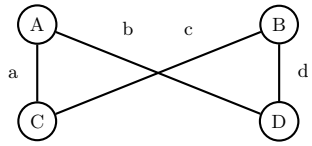

Fig. 4: Multiple input tissues (A and B) against multiple output tissues (C and D).

UniProt[2] [2]. *Neural information retrieval* principles, particularly numerical embeddings of text produced by large language models, are used to identify genes with putative neurotransmission roles. To this end, the similarity of the UniProt description per gene (including the concatenated list of functions) was tested against a simple query containing the terms receptor, brain and neuro. The terms gaba and dopamine were also incorporated in finer-grained queries for a focused selection of genes involved in the dopaminergic and GABAergic systems. Cosine was used as the similarity metric, and the distribution of similarity scores was inspected to select the top genes per query.

3.2 Statistical frame for multi-input *vs* multi-output tissue analysis

The statistical tests introduced can be used to identify regulatory activity that is brain-specific (contrastive against peripheral tissues) or region-specific (differential within brain tissues). Although they can be used to assess differential expression when considering two or more tissues, they are unable to extend this assessment when contrasting multiple input tissues against multiple output tissues, a common procedure when, for instance, contrasting gene expression from multiple brain tissues against multiple peripheral tissues.

To address this challenge, we extend the statistical framework introduced by applying a statistical test at every input tissue, followed by a solid aggregation of estimates. Fig. 4 showcases this scenario, where a represents the p-value acquired from testing differential expression between tissues `A` and `C`, b between tissues `A` and `D`, c between tissues `B` and `C`, and d between tissues `B` and `D`. To test if a given gene is differentially expressed on the two sets of tissues,

$$p\text{-}value_{2\text{v}2} = \min(\max(a, b), \max(c, d)). \tag{1}$$

This aggregate, p-value$_{2v2}$, is statistically sound because: i) $\max(a, b)$ represents the most conservative p-value when testing tissue `A` against both output tissues `C` and `D`; ii) similarly, $\max(c, d)$ is the most conservative p-value when testing tissue `B` against both output tissues; iii) $\min(\max(a, b), \max(c, d))$ selects the strongest evidence of differential expression across all four pairwise comparisons.

This ensures that a gene is only considered differentially expressed if at least one input tissue shows consistent differential expression against both output tissues. Intuitively, this aggregation strategy requires that for a gene to be considered differentially expressed between input and output tissue sets, at least

[2] UniProt website (`https://www.uniprot.org/uniprotkb?query=organism_id%3A10090`)

one input tissue must be significantly different from *all* output tissues. This conservative approach reduces false positives while preserving statistical power.

This aggregate is easily extensible towards statistical comparisons with n input tissues and m output tissues,

$$p\text{-}value_{nvm} = \min(\max(x_{11}, ..., x_{1m}), \max(x_{21}, ..., x_{2m}), ... \max(x_{n1}, ..., x_{nm})), \quad (2)$$

where x_{ij} is the acquired p-value from comparing the expression of a given gene in the input tissue i against the output tissue j.

3.3 Subspace clustering for pattern-centric multi-tissue stances

The previous gene-centric stances are dedicated to produced summaries focused on generating site-specific ranks of genes with high tissue specificity. These summaries are hereby augmented with pattern-centric stances able to identify putative regulatory modules capturing rich relationships across genes and tissues. To this end, subspace clustering tasks are leveraged.

Given a N-way tensor dataset, *subspace clustering* aims at finding *patterns* (tensor substructures) by simultaneously clustering the N axes, where each pattern satisfies specific criteria of homogeneity and statistical significance.

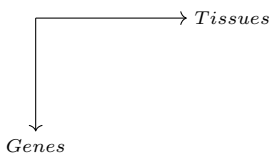

Fig. 5: Biclustering: mapping dimensions.

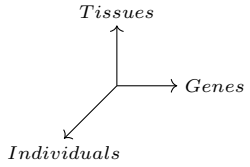

Fig. 6: Triclustering: mapping dimensions.

When N=2, the specialized subspace clustering task is termed **biclustering**. A *bicluster* is a pattern described by a subset of observations (genes) correlated on a subset of variables (tissues) [7]. This organization, presented in Fig. 5, helps us find subsets of genes that exhibit coherent expression patterns across specific subsets of tissues. Each entry in this tensor corresponds to the mean gene expression value in a given tissue across the multiple samples. This work considers three distinct biclustering algorithms: Spectral Coclustering [3], Spectral Biclustering [6], and BicPAMS [4].

When N=3, subspace clustering is termed **triclustering**. A *tricluster* is defined by a set of observations (individuals) correlated on a subset of variables (genes) and contexts (tissues) [5]. This organization, presented in Fig. 6, maps the available expression data into a data cube with the aim at finding groups of individuals that exhibit coherent gene expression signatures across specific tissues (through the z-axis). The TriCluster algorithm, proposed by Zhao and Zaki [11], is selected to flexibly retrieve triclusters with an additive form of coherence, thereby offering the capacity to accommodate shifting factors on gene expression signatures.

4 Visualization Tool

Gene-Centric Tab. Fig. 7 displays the gene-centric tab of the target web-based application, where controlled parameters are marked from `[P1]` to `[P5]`: i) `[P1]` dropdown denotes the tissues in the input set (brain tissues), offering 18 options with no limit on the number of selections; ii) `[P2]` dropdown refers to the tissues in the output set (brain or peripheral tissues) and guarantees that each tissue is mutually exclusive and cannot be used in both the input and output sets; iii) `[P3]` dropdown marks the genes retrieved from automatic gene identification, allowing the user to select one or more genes; iv) `[P4]` dropdown represents different psycho-demographic profiles, e.g., sex, age, and agonal state, with the ability to apply multiple filters; and v) `[P5]` checkbox serves as an alternative for the automatically retrieved genes, enabling the user to utilize pre-established genes related to neurotransmitters of interest in the `[P2]` dropdown, such as those involved in dopaminergic and GABAergic systems retrieved from the STRING initiative [10], a tool that integrates protein-protein interactions.

Fig. 8 and Fig. 9 showcase distinct views, when a single gene or multiple genes are selected, respectively. In Fig. 8, we selected two tissues in the input set (amygdala and cortex), two tissues in the output set (blood and adipose tissue), and a single gene of interest (*GABRR1*). The application provides an interactive heatmap representing the p-values calculated for each combination of

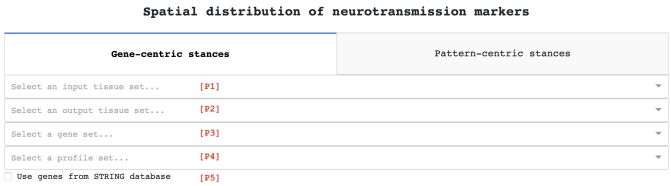

Fig. 7: Gene-centric tab.

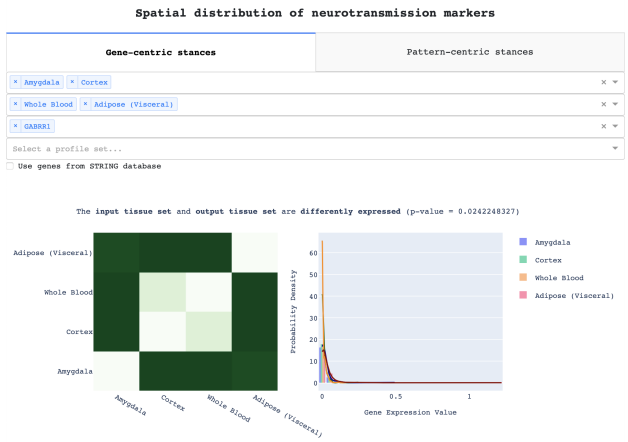

Fig. 8: Webapp view for gene-centric analysis.

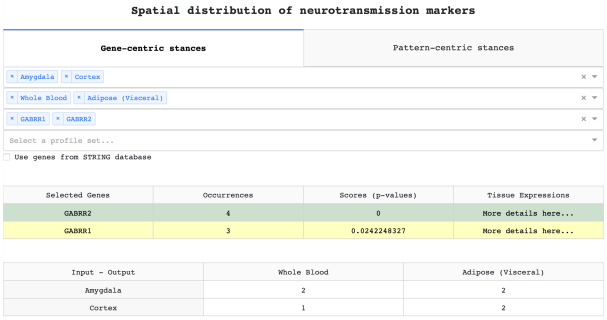

Fig. 9: Webapp view for multiple gene analysis.

tissues, where darker green colors indicate lower p-values, highlighting statistical differences in expression. Additionally, the tool includes an interactive kernel density estimator to show the distribution of the expression values of the selected gene in each chosen tissue. Finally, we provide a textual conclusion on whether the input and output sets exhibit differential expression.

In Fig. 9, we maintained the selected tissues while adding a new gene, *GABRR2*. This figure presents a first table, ordered by p-value, that summarizes information for each gene, including the number of times it is differentially expressed for each combination of tissues, the final calculated p-value for the gene, and the mean and standard deviation of the gene expression for each tissue. The table provides additional details upon clicking each row: (i) the first column displays a kernel density estimator, similar to the view with only one gene; (ii) the third column presents a boxplot with all the p-values used in the calculation of the final p-value (assuming three or more p-values are available); and (iii) the fourth column offers textual information. Furthermore, each row in the table is colour-coded based on the p-value conclusion, ranging from dark green for the lowest p-value to red for the highest. Lastly, we also present a second table (non-clickable) that indicates the number of genes exhibiting differential expression between each combination of input and output tissues.

Pattern-Centric Tab. Fig. 10 displays the results from Spectral Coclustering and Spectral Biclustering, with parameterizations ranging from `[P6]` to `[P8]`: (i) `[P6]` dropdown refers to the algorithm chosen by the user, with options including Spectral Coclustering, Spectral Biclustering, BicPAMS, and TriCluster; (ii) `[P7]` dropdown denotes the tissues selected for the algorithm, where at least two tissues must be chosen to run any algorithm; and (iii) `[P8]` dropdown represents the maximum number of clusters the algorithm should find.

In Fig. 11, we illustrate how BicPAMS is parameterized: (i) `[P9]` dropdown defines the type of desired biclusters, either constant or order-preserving biclusters; and (ii) `[P10]` refers to the mapper strategy to be considered.

In Fig. 12, we illustrate how TriCluster is parameterized: (i) `[P11]` dropdown refers to the minimum size of the triclusters in terms of individuals, with a value between two and the total number of individuals present for the selected tissues;

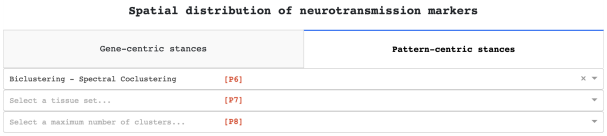

Fig. 10: Pattern-centric tab for spectral coclustering and biclustering.

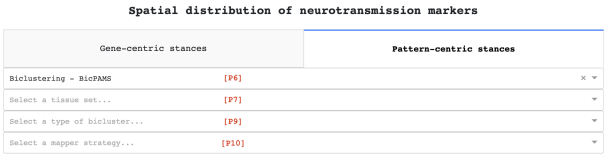

Fig. 11: Pattern-centric tab for the BicPAMS algorithm.

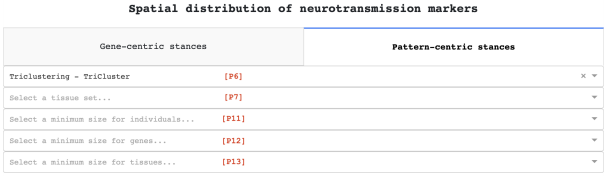

Fig. 12: Pattern-centric tab for the TriCluster algorithm.

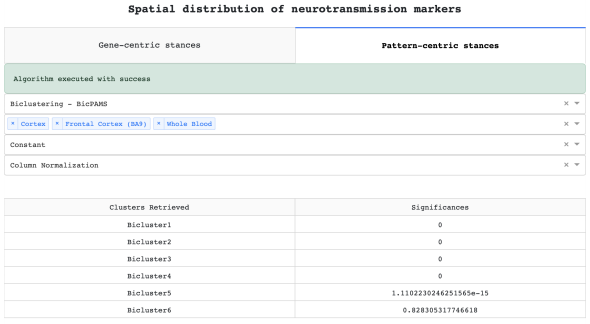

Fig. 13: Webapp view displaying an illustrative BicPAMS solution.

(ii) `[P12]` dropdown represents the minimum size of the triclusters in terms of genes, with a value between two and the maximum number of genes, which is 196; and (iii) `[P13]` dropdown refers to the minimum size of the triclusters in terms of tissues, with a value between two and the number of selected tissues.

For illustrative purposes, we show an example of the application's display after executing BicPAMS' biclustering algorithm in Fig. 13. BicPAMS is applied over three selected tissues (cortex, frontal cortex, and blood) and parameterized to find constant biclusters after performing column-wise normalization. The application provides an interactive table that showcases all the biclusters found, ordered by significance. By clicking on each bicluster, a pop-up opens, displaying the dimensions, row and column labels, and details of the selected bicluster.

5 Results

Gene-Centric Results. The gene-centric assessment of neurotranscriptomic markers is conducted in three stages, corresponding to coarse, intermediary, and fine grained views. First, we assess differential expression of all 56,200 genes supplied by the GTEx initiative between two different groups of tissues – four brain tissues (amygdala, frontal cortex, hippocampus, and hypothalamus) and three peripheral tissues (whole blood, adipose visceral tissue, and skin without sun exposure). Results are depicted in Table 1.

Second, we narrow the scope to 196 automatically retrieved genes focused on the regulation of neurotransmission systems. When assessing the differential analysis between two groups – amygdala and frontal cortex (BA9) versus whole blood – we confirm that most genes (182 out of 196) show high differentiation (brain specificity), yielding p-values lower than 0.001.

Lastly, we turn our focus to the dopaminergic system, specifically analyzing 11 pre-established top genes identified by the STRING portal, assessing whether they are differentially expressed between the amygdala and the frontal cortex (BA9). As depicted in Table 2, 7 (out of the 11) genes show differential expression at α=0.001. We further ascertain the tissue where gene expression is up-regulated, offering insight into the functional role of these genes.

Table 3 identifies the enriched pathways of the up-regulated (activated) genes in the amygdala, confirming they are primarily involved in neurotransmitter transport and dopaminergic synaptic transmission. These genes have a low adjusted p-value for disorders such as social phobia and impulsivity, suggesting a crucial role in emotional regulation and behavioral responses mediated by the amygdala. The enrichment of schizophrenia-related pathways further establishes a putative link between these genes and the disease.

Table 1: Number of differentially expressed genes at brain tissues.

	whole blood	adipose (visceral)	skin (not sun exposed)
amygdala	37,264	36,718	38,079
frontal cortex (BA9)	39,864	38,206	39,623
hippocampus	38,706	37,620	38,950
hypothalamus	39,143	37,731	39,156

Table 2: Differential expression of core genes that regulate the dopaminergic system across brain tissues (amygdala versus frontal cortex).

gene	p-value	regulatory direction
DBH	$< 1\text{E}^{-10}$	Up-regulated (activated) on the frontal cortex (BA9)
DRD5	$< 1\text{E}^{-10}$	Up-regulated (activated) on the frontal cortex (BA9)
DRD2	4.5E^{-9}	Up-regulated (activated) on the amygdala
SLC6A3	9.55E^{-8}	Up-regulated (activated) on the amygdala
DRD3	3.253E^{-5}	Up-regulated (activated) on the frontal cortex (BA9)
SLC6A2	2.015E^{-4}	Up-regulated (activated) on the amygdala
DRD4	2.572E^{-4}	Up-regulated (activated) on the frontal cortex (BA9)
SLC18A2	0.154	
LRTOMT	0.379	
COMT	0.738	
TH	0.933	

Table 3: Enriched terms of up-regulated dopamine-related genes in the amygdala (DRD2, SLC6A3, SLC6A2).

category	description	adjusted p-value
pathways	Na+/Cl- dependent neurotransmitter transporters (Reactome 2022)	4.102E^{-5}
	Dopaminergic synapse (KEGG 2021 Human)	4.735E^{-4}
ontologies	Dopaminergic synaptic transmission and uptake (GO Bio. Process 2023)	7.621E^{-6}
	Monoamine transmembrane transporter (GO Molecular Function 2023)	4.678E^{-6}
diseases	Social phobia (DisGeNET)	1.961E^{-7}
	Impulsive character (DisGeNET)	2.485E^{-6}
	Schizophrenia (DisGeNET)	0.03

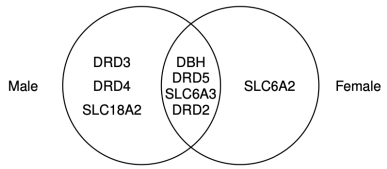

Fig. 14: Dopamine-related genes differentially expressed depending on the sex.

Sex- or age-specific functions within the dopaminergic system can be explored by conditioning the differential analysis to demographic subgroups. Fig. 14 provides a summarized view of the highlighted differences between sexes on the differential expression (amygdala versus frontal cortex) of dopamine-related genes.

Pattern-Centric Results. The pattern-centric stances offered in the visualization tool assisted with the identification of putative multi-tissue regulatory modules (patterns). Specifically, the tool-mediated application of BicPAMs with default parameters over GTEx data retrieved a high number of constant and order-preserving biclusters, with 85% exhibiting statistical significance at α=1E-3. Alternative parameterizations can be explored to expand the initial result set, thereby supporting further knowledge expansion. A closer examination of one of the most statistically significant biclusters, Bic1, described by 62 genes[3] coherently co-expressed on 3 brain tissues – cortex, whole blood, frontal cortex (BA9) –, as highlighted by a low mean squared residue of 0.024.

Conversely, triclustering expands biclustering stances by identifying clusters across three dimensions (sample-gene-tissue). The application of the TriCluster algorithm [11] under the following parameterization — a minimum of 2 individuals at the row level; a minimum of 10 genes at the column level; and a minimum of 9 tissues at the context level — reveals triclusters yielding high statistical significance (p-values below 1E-20). For illustrative purposes, Fig. 15 plots a single tricluster, Tric4, containing two individuals, GTEX-1GN73 and GTEX-1B8L1,

[3] *ACVR1C, ADGRF3, CCDC62, CCKAR, CLEC4M, DBH, DDC, DRD2, DRD5, GABRA6, GABRB1, GABRE, GABRG3, GABRQ, GALR1, GLP2R, GPR148, GPR149, GPR45, GPR52, GPR63, HTR1A, HTR1B, KLHL1, MC5R, P2RY6, PCDHA1, PCDHA10, PCDHA11, PCDHA12, PCDHA13, PCDHA2, PCDHA3, PCDHA5, PCDHA6, PCDHA8, PCDHA9, PCDHAC1, PCDHB11, PCDHB12, PCDHB13, PCDHB15, PCDHB16, PCDHB2, PCDHB3, PCDHB7, PCDHB9, PCDHGA1, PCDHGA2, PCDHGA4, PCDHGA5, PCDHGA6, PCDHGA7, PCDHGA10-11, PCDHGB1, PCDHGB3, PCDHGB4, PCDHGB5, PCDHGB6, RANBP17, RGS17*

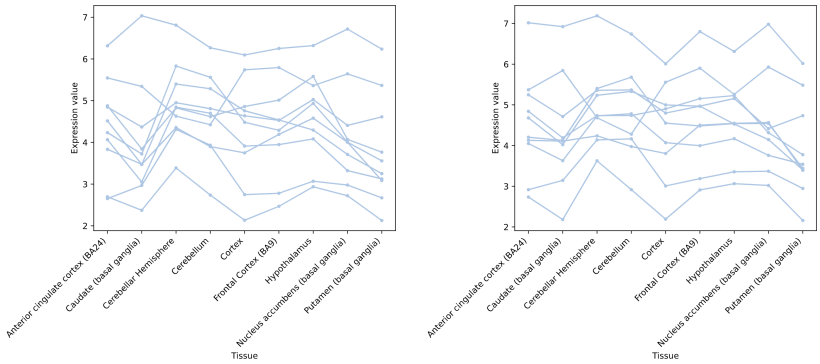

(a) individual GTEX-1B8L1 (b) individual GTEX-1GN73

Fig. 15: Additive pattern (tricluster Tric4) with the expression signature of 10 genes across 9 brain tissues for two individuals.

corresponding to male individuals with ages in the range 60-69 and an agonal state of fast death from natural causes. The captured genes satisfy an additive coherence over the selected tissues, suggesting a putative regulatory dynamic.

The *associative strength* between patterns and covariates of interest can be explored in order to study multi-tissue regulatory activity that is discriminatively observed on specific psycho-demographic groups. Some of the retrieved patterns yield strong dependencies with specific covariate categories as determined by high lift scores, an indicator of the strength of an association against expectations. Illustrating, the lift of the association between Tric4 pattern and the population subgroup of males aged 60-69 with a fast death from natural causes is 11.083, i.e., this putative regulatory module (describe by an expression program spanning 10 genes and 9 brain tissues) is 11 times more likely to be associated with this demographic-and-agonal subgroup than what would be expected by random chance.

The putative regulatory patterns unraveled by biclustering and triclustering searches can be further subjected to functional enrichment analysis, similarly to gene-centric stances (e.g., Table 3). This exploration is of critical relevance to assess their putative roles in key biological processes and pathways, thereby contributing to the actionability of the target maps.

6 Conclusion

This work introduced a web-based visualization tool for learning neurotranscriptomic maps that describe spatial distribution of neurotransmission markers in the brain using statistical frameworks for differential expression analysis. Users can contrast brain-to-brain and brain-to-peripheral tissues while incorporating demographic and clinical co-factors. The tool enables focused exploration of specific gene families and neurotransmission pathways, while supporting the discovery of putative regulatory modules (patterns) through biclustering stances

(co-expressed genes across tissues) and triclustering stances (groups of individuals with coherent multi-tissue gene expression). Results confirm the tool's effectiveness in guiding knowledge expansion through interactive map exploration and functional enrichment analyses.

Key future directions include extending the approach for other omics and organisms; integrating clinical data to assess how transcriptional signatures are altered in the context of specific diseases and psychotropic drug action; and enhancing interactive visualizations for improved usability.

Acknolwedgments. This work was supported by Fundação para a Ciência e a Tecnologia through AIpALS (PTDC/CCI-CIF/4613/2020), FRAIL (2024.07266.IACDC), and LAIfeBlood+ (2024.07475.IACDC) projects; INESC-ID pluriannual (UIDB/50021/2020); LASIGE Research Unit (UID/000408/2025); and scholarship to M. Moreira.

References

1. Carithers, L.J., Moore, H.M.: The genotype-tissue expression (gtex) project. Biopreservation and biobanking **13**(5), 307 (2015)
2. Consortium, T.U.: Uniprot: the universal protein knowledgebase in 2023. Nucleic Acids Research, Volume 51, Issue D1, Pages D523–D531 (2023)
3. Dhillon, I.S.: Co-clustering documents and words using bipartite spectral graph partitioning. ACM SIGKDD p. 269–274 (2001)
4. Henriques, R., Ferreira, F.L., Madeira, S.C.: Bicpams: software for biological data analysis with pattern-based biclustering. BMC Bioinformatics (2017) 18:82 (2017)
5. Henriques, R., Madeira, S.C.: Triclustering algorithms for three-dimensional data analysis: A comprehensive survey. ACM Computing Surveys, Vol. 51, No. 5, Article 95 (2018)
6. Kluger, Y., Basri, R., Chang, J.T., Gerstein, M.: Spectral biclustering of microarray data: coclustering genes and conditions. Genome research, 13(4):703–716 (2003)
7. Madeira, S.C., Oliveira, A.L.: Biclustering algorithms for biological data analysis: A survey. IEEE Trans. Comput. Biology and Bioinf., Vol. 1, No. 1 (2004)
8. Mahfouz, A., Huisman, S.M.H., Lelieveldt, B.P.F., Reinders, M.J.T.: Brain transcriptome atlases: a computational perspective. Brain Struct Funct. 2017; 222(4): 1557–1580 (2017)
9. Ortiz, C., Carlén, M., Meletis, K.: Spatial transcriptomics: Molecular maps of the mammalian brain. Annual Review of Neuroscience pp. 547–562 (2021)
10. Szklarczyk, D., Kirsch, R., Koutrouli, M., Nastou, K., Mehryary, F., Hachilif, R., Gable, A.L., Fang, T., Doncheva, N.T., Pyysalo, S., Bork, P., Jensen, L.J., von Mering, C.: The string database in 2023: protein-protein association networks and functional enrichment analyses for any sequenced genome of interest. Nucleic Acids Research, Volume 51, Issue D1, Pages D638–D646 (2023)
11. Zhao, L., Zaki, M.J.: Tricluster: an effective algorithm for mining coherent clusters in 3d microarray data. ACM SIGMOD p. 694–705 (2005)